# Ruthenium carbamoyl complexes: coordination chemistry and CO release

Mark A. Wright[a], Maria A. O'Connell[b], Joseph A. Wright[a,*]

[a]*Energy Materials Laboratory, School of Chemistry, University of East Anglia, Norwich Research Park, Norwich, NR4 7TJ, United Kingdom*
[b]*School of Pharmacy, University of East Anglia, Norwich Research Park, Norwich, NR4 7TJ, United Kingdom*

## 1. Introduction

The coordination chemistry of first-row transition metal carbonyl complexes is attracting increasing attention due to their potential as therapeutics [1–7]. Exogenous carbon monoxide has over the past two decades been shown to have useful applications as an anti-inflammatory [8] and in neurodegenerative and cardiovascular diseases [9]. The release of CO by first-row transition metal carbonyls can be stimulated by irradiations with visible- or near-UV light, thus offering a controlled delivery method for CO. Used in this way, so-called photoCORM (CO-releasing molecules) may provide a novel route to delivering an otherwise highly-toxic gas.

We have recently reported photoCORM behaviour of a series of ferracyclic carbonyl complexes and explored their activity as anti-inflammatory agents *in vitro* [10]. There have also been a small number of other reports of photoCORM activity from iron-based systems [11–15], whilst the greatest focus of research to date has centred on Mn(I) systems [16–33].

Work on the heavier transition metals has been much more limited, not least because they primary absorb only in the UV and thus have more limited therapeutic potential. Thermally-activated ruthenium-based CORM are some of the longest-known systems [13]. Photochemically-activated rhenium and ruthenium complexes have been explored either as potential photoCORM in their own right [28, 34–38], or as models for the release behaviour of more active systems [39]. The latter aspect, together with a more fundamental desire to probe the coordination chemistry of the carbamoyl moiety, promoted us to extend our earlier Fe(II) study to the chemistry of Ru(II) carbonyls.

## 2. Results and discussion

### *2.1. Synthesis*

Early work by Nonoyama [40] has more recently been followed by Leong and co-workers, who have reported a series of ruthenium carbamoyl complexes as analogues of the [Fe]-hydrogenase [41, 42]. Our synthetic path is similar, though

*Corresponding author

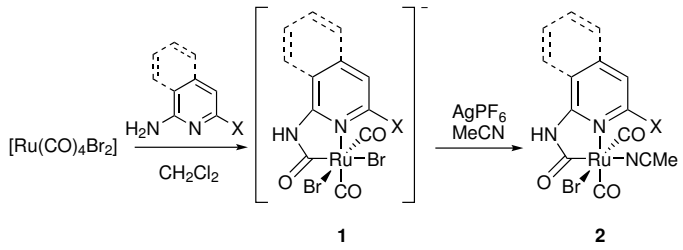


**1** **2**

Figure 1: Synthesis of complexes **1** and **2**; **a** X = H, pyridyl; **b** X = H, isoquinyl; **c** X = $NH_2$, pyridyl; **d** X = $NH_2$, isoquinyl.

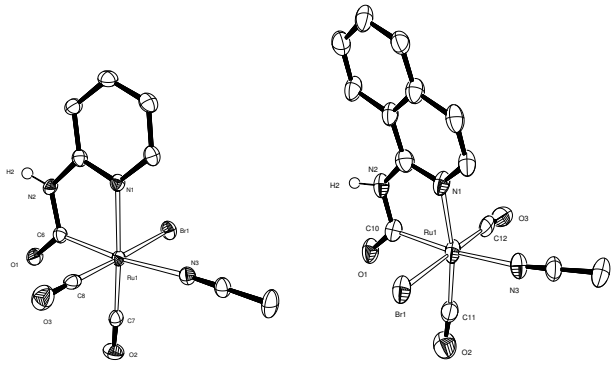


Figure 2: ORTEP representation of the structures of **2a** · MeCN (left) and **2b** · MeCN (right) showing 50 % probability ellipsoids; solvent molecules and hydrogen atoms attached to carbon have been omitted for clarity.

in our hands some variations were required. As reported by Leong, reaction of $Ru(CO)_4Br_2$ with 2-aminopyridine (Figure 1) in dried dichloromethane resulted in the evolution of CO gas and rapid formation of a white precipitate. X-ray diffraction confirmed this was the anticipated salt **1** (Figure S7). The precipitate could be redissolved in the coordinating solvent, acetonitrile. However, in contrast to the iron system and the route reported by Leong, in our hands this did not result in formation of the neutral solvent adduct. To bring about loss of a halide from the metal centre, $AgPF_6$ was added, leading smoothly to the target complex **2a**. Isolation of the isoquinoline derivative **2b** followed an identical reaction pathway. X-ray quality crystals were isolated upon cooling the reaction solutions, and confirmed the desired coordination geometry (Figure 2). Bond lengths of the in **2a** are typically around 0.1 Å longer than for the iron structure (Table 1), consistent with the larger size of the heavier metal centre. For complex **2b**, there is more variability in the expansion caused by the move from iron to ruthenium, though the overall pattern remains. Notably, both in **2b** and the iron analogue, the C=O bond length for one of the bound CO molecules is significantly shortened compared with the pyridyl systems, presumably due to poorer donation by the isoqunioyl nitrogen atom.

The IR profile of **2b** in solution shows the characteristic peak pattern seen previously for **2a** and the iron systems: three carbonyl peaks at 2061 $cm^{-1}$,

Table 1: Comparison of metrical data for **2a**·MeCN, **2b**·MeCN and their ferracyclic analogues [10]

| | Bond distance/Å | | | |
|---|---|---|---|---|
| | Complex **2a** | | Complex **2b** | |
| | Iron | Ruthenium | Iron | Ruthenium |
| M−Br | 2.4632(5) | 2.5612(3) | 2.4585(5) | 2.5549(15) |
| M−C(6) | 1.931(2) | 2.012(2) | 1.942(3) | 2.044(10) |
| M−C(7) | 1.782(3) | 1.884(3) | 1.796(3) | 1.913(11) |
| M−C(8) | 1.811(3) | 1.910(3) | 1.915(5) | 1.984(15) |
| M−N(1) | 1.992(2) | 2.112(2) | 1.998(3) | 2.128(9) |
| M−N(3) | 2.022(2) | 2.187(2) | 2.025(3) | 2.194(9) |
| C(6)−O(1) | 1.229(3) | 1.236(3) | 1.227(4) | 1.224(12) |
| C(7)−O(2) | 1.136(3) | 1.137(3) | 1.130(4) | 1.115(13) |
| C(8)−O(3) | 1.086(3) | 1.089(3) | 0.901(4) | 0.927(14) |

2000 $cm^{-1}$ and 1991 $cm^{-1}$ and two carbamoyl signals at 1667 $cm^{-1}$ and 1631 $cm^{-1}$. Comparison for the positions of the carbonyl vibrational bands of the iron and ruthenium complexes reveal the latter reside at a much higher wavenumber in both **2a** and **2b**. The strengthened carbon–oxygen bonds of the ruthenium carbonyls suggest a weakened M−C bond and increased labilisation of CO. Indeed, the larger 4d molecular orbitals of the ruthenium metal centre participates in less efficient overlap with the $\pi^*$ orbital of the CO ligand, whereas the iron complexes participate in stronger back-donation due to the more efficient overlap of the 3d molecular orbitals. This is a distinct advantage of designing ruthenium-based CORM over iron-based CORM.

Incorporation of additional heteroatoms either into the aromatic backbone or as conjugated substituents is one pathway to enhanced light sensitivity. The simple heterocycle 2,6-diaminopyridine is commercially available, whereas 1,3-diaminoisoquinoline was synthesised according to the literature procedure [43]. Reaction between these heterocycles and $Ru(CO)_4Br_2$ proceed smoothly, yielding first the intermediate salts, then after treatment with $AgPF_6$/MeCN the target molecules **2c** and **2d** (Figures 1 and 3). Both complexes bear the characteristic five-membered metallocyclic ring, with bound *cis* dicarbonyl ligands. However, the occupation of the sixth ligand (*trans* to the carbamoyl linkage) of **2d** is unique: the bromide ligand occupies the sixth position, with the solvent ligand *trans* to CO. This allows formation of an intramolecular $NH_2\cdots Br$ hydrogen bond, absent in **2c**. Metrical data (Table 2) show that, as would be expected, placing the bromide *trans* to the carbamoyl elongates the Ru−Br bond, whilst the bound acetonitrile is coordinated more closely. Notably, the very short C−O bond seen in **2b** is *absent* in these systems.

The IR spectra for **2c** and **2d** confirmed the *cis* carbonyl geometry is maintained in solution (2066 $cm^{-1}$ and 2003 $cm^{-1}$ for **2c**, 2065 $cm^{-1}$ and 2003 $cm^{-1}$ **2d**). There is a small but clear strengthening of the C≡O bond in **2c** and **2d**. This could be a consequence of reduced back-donation, implying that the $NH_2$-substituted ligands are poorer electron donors to the metal. The ability of the ligand to donate to the metal depends on the availability of electron density in the pyridyl lone pair, and this may be reduced by the inductive effect of the $NH_2$-substituent.

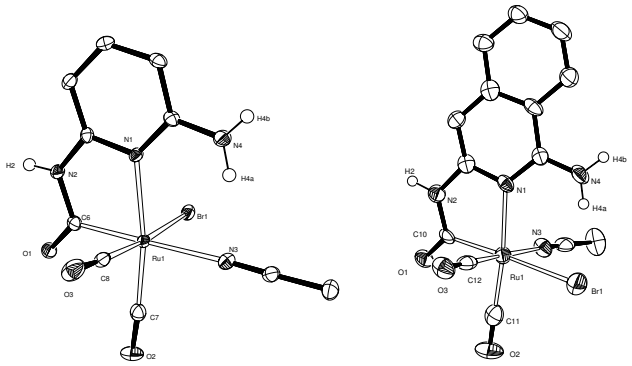


Figure 3: ORTEP representation of the structures of **2c** (left) and **2d** · MeCN (right) showing 50 % probability ellipsoids; solvent molecules and hydrogen atoms attached to carbon have been omitted for clarity.

Table 2: Comparison of metrical data for **2c** and **2d** · MeCN.

| | Bond distance/Å | |
|---|---|---|
| | Complex **2c** | Complex **2d** |
| M−Br | 2.5695(5) | 2.6799(11) |
| M−C(6) | 2.013(4) | 2.049(9) |
| M−C(7) | 1.892(4) | 1.890(9) |
| M−C(8) | 1.881(5) | 1.876(9) |
| M−N(1) | 2.167(3) | 2.164(6) |
| M−N(3) | 2.213(4) | 2.114(7) |
| C(6)−O(1) | 1.226(5) | 1.213(9) |
| C(7)−O(2) | 1.138(6) | 1.134(10) |
| C(8)−O(3) | 1.131(6) | 1.138(9) |

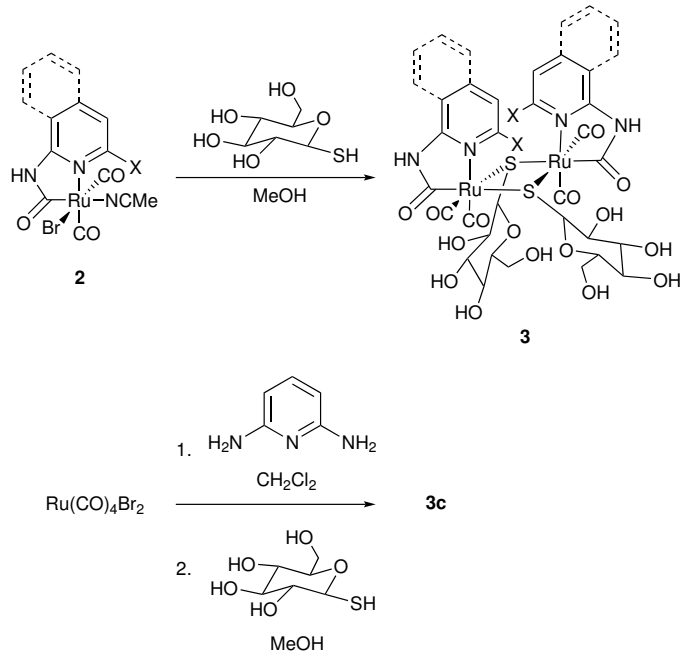


Figure 4: Synthesis of complex **3**; **a** X = H, pyridyl; **b** X = H, isoquinyl; **c** X = $NH_2$, pyridyl; **d** X = $NH_2$, isoquinyl.

To enhance the water solubility and biocompatibility of the ruthenium carbonyls, we replicated the introduction of a thiolated saccharide ligand in the same way as explored for iron. Introduction of the monosaccharide by reaction with the halides **2** yielded dimeric structures analogous to the iron complexs, which was confirmed by X-ray crystallography for **3b** (Figure 5). In the case of **3c**, direct reaction with the intermediate salt **1c** was possible, allowing omission of the halide abstraction step.

Metrical data (Table 3) again show the elongated bonding around the 4d metal. The IR spectra of these thiolated complexes exhibited a characteristic shift in carbonyl bands to lower wavenumber.

*2.2. UV/visible spectra and CO release*

Examination of the electronic spectra for **2a** and **2b** in DMSO reveal that neither complex display absorbance bands in the visible region (Figure 6). Unsurprisingly, attempts to release CO from these solutions using visible light were unsuccessful. However, when exposed to UV irradiation, rapid loss of the carbonyl bands was seen in the IR spectra; in contrast, extended storage (hours) of the solutions in the dark did not lead to appreciable degradation.

Introduction of the additional amino functional group onto the ligand architecture produced a marked increased in the absorption band at 340 nm in **2c**. The combination of the extended conjugation system and presence of an additional donor functional group results in **2d** displaying an absorption band in the visible region of the spectrum. Despite the notable absorbance peak above 400 nm, investigations using IR spectroscopy and the myoglobin assay revealed no liberation of CO under visible light irradiation.

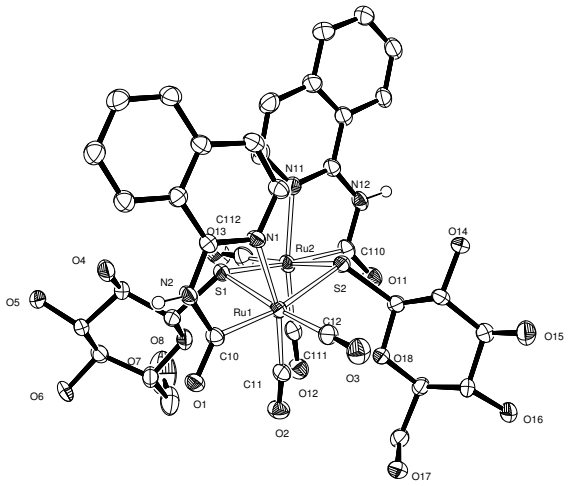


Figure 5: ORTEP representation of the structure of **3b** $\cdot 1.5(H_2O) \cdot 3\,(MeOH)$ showing 50 % probability ellipsoids; solvent molecules and hydrogen atoms other than those on nitrogen have been omitted for clarity.

Table 3: Comparison of metrical data for **3b** $\cdot 1.5(H_2O) \cdot 3\,(MeOH)$ and the ferracyclic analogue [10].

| | Bond distance/Å | |
|---|---|---|
| | Iron | Ruthenium |
| M(1)−S(1) | 2.372(3) | 2.4423(14) |
| M(1)−N(1) | 2.019(5) | 2.124(5) |
| M(1)−C(10) | 1.926(5) | 2.020(5) |
| M(1)−C(11) | 1.786(6) | 1.898(6) |
| M(1)−C(12) | 1.782(7) | 1.902(6) |
| C(10)−O(1) | 1.239(6) | 1.245(6) |
| C(11)−O(2) | 1.136(7) | 1.132(7) |
| C(12)−O(3) | 1.135(8) | 1.125(8) |

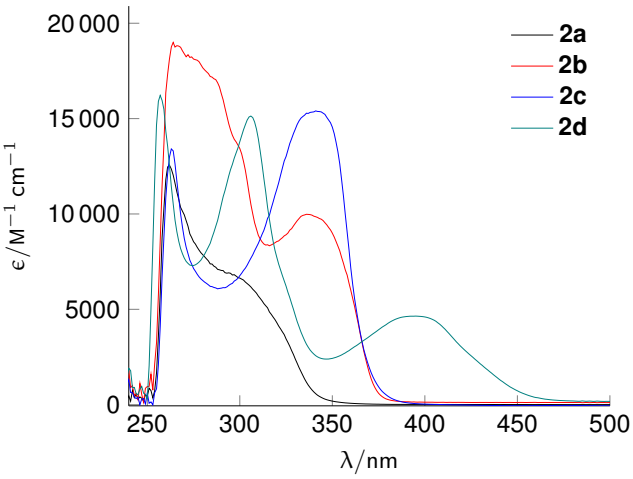


Figure 6: Electronic absorption spectra of **2a**–**2d** in DMSO.

Moving to the dimeric glucose-containing series (Figure 7), absorption maxima remained largely in the UV region with the exception of complex **3d**. In contrast to **2d**, the latter did exhibit loss of CO when exposed to broad-band visible light, as assessed by monitoring of the IR spectrum of the reaction (Figure S8). CO release from this system was probed further in a myoglobin assay (Figure 8). Here, under high-power light (0.840 W), two equivalents of CO were released per metal centre, whilst with lower power irradiation (0.216 W) only a single CO was liberated. This contrasted with the iron homologues, where two CO molecules were released in all cases [10]. It is not clear what the source of this lowered reactivity is: no by-products could be isolated from solution, and thus it is unclear if the effect is due to release of a single CO or of a lower number of molecules decomposing.

### *2.3. Anti-inflammatory assays*

As reported previously, whilst ferracyclic carbamoyl complexes release CO in the light, they are only effective as anti-inflammatory agents in the dark [10]. We therefore explored the potential of complex **2a** in an assay of the inhibitory effect on lipopolysaccharide-induced tumour necrosis factor-alpha (TNF) secretion in human THP-1 monocytes [44], reasoning that some activity might arise even without quantifiable CO release in the light. The assay has previously been established as an *in vitro* model for inflammation response [45].

Disappointingly, **2a** (50 μM) caused a marginal response in the assay in the dark (Figure S9), under the same conditions which had been successful for the iron systems [10]. As expected, visible light stimulation had no bearing on the degree of activity observed. This behaviour contrasts markedly with the ferracyclic system, and further exploration in this area was not pursued.

## 3. Conclusions

In conclusion, a series of Ru(II) carbamoyl complexes have been synthesised using a modification of the protocols previously employed for ferracyclic sys-

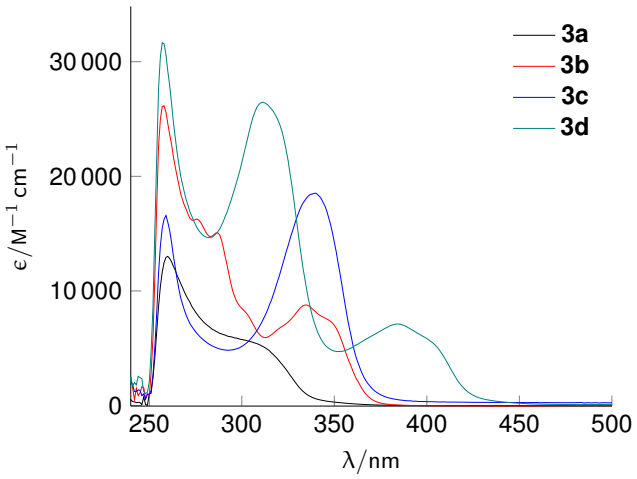


Figure 7: Electronic absorption spectra of **3a**–**3d** in DMSO.

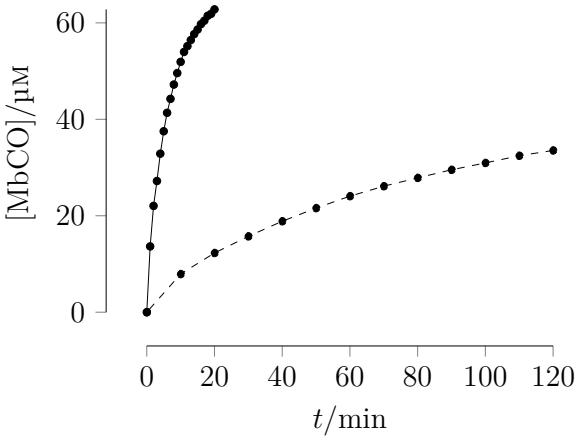


Figure 8: Plot of the amount of MbCO formed *via* CO liberated from **3d** (30 μM) (Dashed and solid lines represent low and high power light output, respectively.)

tems. Metrical data shows that the iron and ruthenium complexes are structurally similar but the latter have metal–ligand bonds elongated by around 0.1 Å. The ruthenium complexes are light-stable but release CO under UV irradiation. Unlike the iron systems, no activity was seen in an anti-inflammatory assay either in the light or the dark. These complexes therefore offer the potential to act as stable models for their more active iron homologues.

## 4. Experimental

### *4.1. General*

All reactions were conducted under a dry nitrogen atmosphere using standard Schlenk techniques. Starting materials were purchased from Aldrich or Alfa Aesar and were used without further purification. All glassware and solvents were pre-dried and degassed prior to use. The appropriate drying agents were used for solvent drying: $CH_2Cl_2$ ($CaH_2$), tetrahydrofuran ($Na/(C_6H_5)_2CO$) and acetonitrile ($CaH_2$). FT-IR spectra were recorded using a Perkin-Elmer SpectrumBX instrument. UV-visible spectra were recorded using an Agilent Technologies Cary 60 in disposable 1 cm plastic cuvettes. Elemental analysis was carried out at London Metropolitan University. NMR spectra were obtain on a Bruker AvanceIII with a nominal proton value of 500 MHz. Mass spectrometry was carried out at the National Mass Spectrometry Facility at the Swansea University. The preparations of 1,3-diaminoisoquinoline [43] and 1-thio-β-D-glucose [48] were carried out following literature procedures. The myoglobin and TNF assay protocols have been reported previously [10]. Light irradiation was carried out using a UV TLC illuminator or Krüss Optronic visible lamp (230 V, 150 W) at two light intensities: 0.216 W and 0.840 W.

### *4.2. $Ru(CO)_4Br_2$*

The route used was modified from the literature [46, 47]. Thus $Ru_3(CO)_3$ (100 mg, 0.15 mmol) was suspended in dry heptane (100 $cm^3$), and the vessel filled with CO. The stirred solution was irradiated with a 455 nm LED for 75 minutes, after which time a light yellow solution had formed. This was cooled to −40 °C before addition of $Br_2$ (0.04 $cm^3$, 0.78 mmol) in heptane (20 $cm^3$). After warming to room temperature, the resulting solid was recovered by filtration and used without further purification.

### *4.3. Complex **2a***

To a solution of $Ru(CO)_4Br_2$ (50 mg, 0.13 mmol) in $CH_2Cl_2$ (10 $cm^3$) was added 2-aminopyridine (27 mg, 0.29 mmol). Gas was evolved and a white precipitate formed almost immediately. Once precipitation was complete, the supernatant was removed *via* decantation. The white product was redissolved in acetonitrile. Addition of one equivalent of $AgPF_6$ under stirring resulted in the formation of AgBr precipitation. Filtration and cooling of the solution yielded colourless X-ray quality crystals of $RuBr(C_6H_5N_2O)(CO)_2(MeCN)$ (36 mg, 49 %). $T_m$ 167 °C. Found C 30.23, H 1.99, N 10.44 %; $C_{10}H_8BrN_3O_3Ru$ requires C 30.09, H 2.02, N 10.53 %. UV/Vis (DMSO) $\lambda_{max}$ 298 ($6.74 \times 10^3$), 262 ($1.26 \times 10^4$) nm ($M^{-1}\,cm^{-1}$). $\tilde{\nu}_{max}$ (THF) 2055, 1987, 1672, 1621 $cm^{-1}$. $^1H$ NMR ($CD_3CN$, 500 MHz) 1.96 (s, 6H, Me), 7.02 (m, 4H, py), 7.84 (m, 2H, py), 8.37 (ddd, $J$ = 0.9, 1.5, 5.8 Hz, 1H, py), 8.58 (br s, 1H, NH), 8.76 (br s, 1H,

NH), 9.08 (ddd, $J$ = 0.9, 1.5, 1H, 5.8 Hz, py). $^{13}$C NMR ($CD_3CN$, 126 MHz) 110.25, 110.43, 117.43, 117.72, 141.57, 142.07, 148.39, 149.43. $m/z$ (orbitrap) 319.9 $[M - Br]^+$.

### *4.4. Complex **2b***

The reaction was carried out as for **2a** using $Ru(CO)_4Br_2$ (54 mg, 0.14 mmol) and 1-aminoisoquinoline (48 mg, 0.33 mmol), yielding colourless crystals of $RuBr(C_{10}H_7N_2O)(CO)_2(MeCN)$ (37 mg, 58 %). $T_m$ 202 °C (dec.). Found C 37.25, H 2.12, N 9.27 %; $C_{14}H_{10}BrN_3O_3Ru$ requires C 37.45, H 2.24, N 9.35 %. UV/Vis (DMSO) $\lambda_{max}$ 268 ($1.87 \times 10^4$), 341 ($9.85 \times 10^3$) nm ($M^{-1}\,cm^{-1}$). $\tilde{\nu}_{max}$ (MeCN) 2062, 1994, 1664 $cm^{-1}$. $^1$H NMR ($CD_3CN$, 500 MHz) 1.97 (s, 6H, Me), 6.13 (ddd, 2H, $J$ = 1.1, 8.0, 10.6 Hz, py), 7.42 (t, 1H, $J$ = 8.0 Hz, py), 8.52 (br s, 1H, NH). $^{13}$C NMR ($CD_3CN$, 126 MHz) 95.73, 97.45, 102.18, 141.85, 146.47, 152.99, 163.13. $m/z$ (orbitrap) 369.9 $[M - Br]^+$.

### *4.5. Complex **2c***

The reaction was carried out as for **2a** using $Ru(CO)_4Br_2$ (78 mg, 0.21 mmol) and 2,6-diamisoquinoline (51 mg, 0.47 mmol), yielding colourless crystals of $RuBr(C_6H_7N_3O)(CO)_2(MeCN)$ (44 mg, 52 %). $T_m$ 185 °C (dec.). Found C 28.91, H 2.28, N 13.57 %; $C_{10}H_9BrN_4O_3Ru$ requires C 29.00, H 2.19, N 13.53 %. UV/Vis (DMSO) $\lambda_{max}$ 264 ($1.33 \times 10^4$), 343 ($1.54 \times 10^4$) nm ($M^{-1}\,cm^{-1}$). $\tilde{\nu}_{max}$ (MeCN) 2066, 2002, 1657 $cm^{-1}$. $^1$H NMR ($CD_3CN$, 500 MHz) 9.49 (s, 1H, NH), 8.23–8.17 (m, 2H), 8.13 (d, $J$ = 6.6 Hz, 1H), 8.09–7.82 (m, 4H), 7.78 (dddd, $J$ = 20.3, 8.3, 7.0, 1.3 Hz, 2H), 7.51 (t, $J$ = 6.8 Hz, 3H), 7.24 (dd, $J$ = 7.1, 0.9 Hz, 1H). $m/z$ (orbitrap) 334.9 $[M - Br]^+$.

### *4.6. Complex **2d***

The reaction was carried out as for **2a** using $Ru(CO)_4Br_2$ (90 mg, 0.24 mmol) and 2,6-diaminopyridine (86 mg, 0.54 mmol), yielding colourless crystals of $RuBr(C_{10}H_8N_2O)(CO)_2(MeCN)$ (39 mg, 35 %). $T_m$ 194 °C (dec.). Found C 36.04, H 2.23, N 11.94 %; $C_{14}H_{11}BrN_4O_3Ru$ requires C 36.22, H 2.39, N 12.07 %. UV/Vis (DMSO) $\lambda_{max}$ 258 ($1.60 \times 10^4$), 308 ($1.48 \times 10^4$), 401 ($4.58 \times 10^{43}$) nm ($M^{-1}\,cm^{-1}$). $\tilde{\nu}_{max}$ (MeCN) 22085, 2025, 1675, 1631 $cm^{-1}$. $m/z$ (orbitrap) 486.8938 $[M + Na]^+$.

### *4.7. Complex **3a***

To a solution of **2a** (12 mg, 0.03 mmol) in MeOH (10 $cm^3$ was added one equivalent of 1-thio-β-D-glucose from a stock solution of known concentration. The reaction was allowed to stir for 90 min. The solvent was removed under vacuum yielding a yellow solid (11 mg, 40 %). $T_m$ 194 °C. UV/Vis (DMSO) $\lambda_{max}$ 261 ($1.38 \times 10^4$) nm ($M^{-1}\,cm^{-1}$). $\tilde{\nu}_{max}$ (MeOH) 2064, 1988, 1624 $cm^{-1}$. $^1$H NMR ($d$-$_4$−MeOD, 500 MHz) 2.96 (dd, $J$ = 9.4, 8.7 Hz, 1H, sugar), 3.10 (t, $J$ = 9.0 Hz, 1H, sugar), 3.31 (t, $J$ = 9.0 Hz, 1H, sugar), 3.50–3.41 (m, 2H, sugar), 3.73–3.52 (m, 2H, sugar), 4.01–3.89 (m, 2H, sugar), 4.07 (dd, $J$ = 11.7, 3.4 Hz, 1H, sugar), 4.14 (dd, $J$ = 12.0, 2.6 Hz, 1H, sugar), 4.25 (dd, $J$ = 18.4, 9.3 Hz, 2H, sugar), 6.74–6.64 (m, 1H, py), 6.76 (d, $J$ = 8.7 Hz, 1H, py), 6.85 (ddd, $J$ = 7.2, 5.8, 1.2 Hz, 1H, py), 6.90 (ddd, $J$ = 7.2, 5.8, 1.2 Hz, 1H, py), 7.25–7.12 (m, 2H, py), 7.97–7.82 (m, 2H, py), 8.48 (ddd, $J$ = 5.8, 1.7, 0.8 Hz, 1H, py), 8.56 (ddd, $J$ = 5.9, 1.7, 0.8 Hz, 1H, py). $^{13}$C NMR ($d$-$_4$−MeOD,

126 MHz) 62.55 ($CH_2$), 63.50 ($CH_2$), 70.69, 72.50, 76.41, 77.48, 79.22, 79.26, 82.04, 82.58, 83.90, 87.23, 110.83, 111.02, 111.20, 113.86, 117.54, 117.78, 118.17, 141.25, 141.54, 149.82, 150.33, 159.37, 159.55, 193.28 (CO), 194.05 (CO), 201.84 (CO), 202.27 (CO), 210.30 (CO), 211.60 (CO). $m/z$ (orbitrap) 948.9 $[M+H]^+$.

### *4.8. Complex **3b***

The reaction was carried out as for **3a** using **2b** (3.8 mg, 27 μmol), yielding colourless prisms of the product (2.2 mg, 26 %). Found C 40.92, H 3.33, N 5.29 %; $C_{36}H_{36}N_4O_{16}Ru_2S_2$ requires C 41.30, H 3.47, N 5.35 %. UV/Vis (DMSO) $\lambda_{max}$ 259 ($3.15 \times 10^4$), 338 ($1.10 \times 10^4$) nm ($M^{-1}\,cm^{-1}$). $\tilde{\nu}_{max}$ (MeCN) 2062, 1986, 1662 $cm^{-1}$. $m/z$ (orbitrap) 1048.9 $[M+H]^+$.

### *4.9. Complex **3c***

To a solution of $Ru(CO)_4Br_2$ (110 mg, 0.29 mmol) dissolved in $CH_2Cl_2$ (10 $cm^3$) was added 2,6-diaminopyridine (60 mg, 0.6 mmol) drop-wise at −40 °C. The solution was left to react until it reached room temperature. Once a white precipitation was complete, the supernatant was removed *via* decantation. The solid was dissolved in methanol (10 $cm^3$) and one equivalent of 1-thio-β-D-glucose was added from a stock solution of known concentration. The solution was allowed to react for 90 min, after which the solvent was removed to give a white solid (50 mg, 18 %). Found C 34.18, H 3.31, N 8.43 %; $C_{29}H_{34}N_5O_{16}Ru_2S_2$ requires C 34.43, H 3.51, N 8.60 %. UV/Vis (DMSO) $\lambda_{max}$ 258 ($1.63 \times 10^4$), 342 ($1.82 \times 10^4$) nm ($M^{-1}\,cm^{-1}$). $\tilde{\nu}_{max}$ (MeOH) 2062, 1992, 1664 $cm^3$. $^1$H NMR ($d$-$_4$−MeOD, 500 MHz) 3.38–3.54 (4H, m), 3.69 (2H, dddd, $J$ = 2.9, 5.3, 11.8, 14.4 Hz), 3.82–3.95 (2H, m), 4.26 (1H, d, $J$ = 9.6 Hz), 4.34 (1H, d, $J$ = 2.4, 9.4 Hz), 4.42 (1H, d, $J$ = 9.6 Hz), 4.57 (1H, d, $J$ = 2.0, 9.2 Hz), 6.88 (1H, dd, $J$ = 1.0, 6.1 Hz, 7.19 (1H, ddd, $J$ = 0.9, 5.2, 6.5 Hz), 7.41 (1H, ddd, $J$ = 1.4, 6.8, 8.3 Hz), 7.50–7.58 (2H, m), 7.59–7.64 (2H, m), 7.67 (1H, dddd, $J$ = 1.1, 6.1, 7.1, 8.2 Hz), 7.73–7.81 (1H, m), 7.99 (1H, dd, $J$ = 1.0, 8.4 Hz), 8.15–8.22 (1H, m). $^{13}$C NMR ($d$-$_4$−MeOD, 126 MHz) 63.89 ($CH_2$), 73.14, 79.49, 80.87, 82.42,86.95, 92.10, 112.96, 119.89, 125.31, 127.84, 128.41, 132.26, 139.55, 141.54. $m/z$ (orbitrap) 977.9 $[M]^+$.

### *4.10. Complex **3d***

The reaction was carried out as for **3a** using **2b** (12 mg, 0.026 mmol), yielding a yellow solid (17 mg, 61 %). Found C 39.14, H 3.46, N 7.56 %; $C_{36}H_{38}N_6O_{16}Ru_2S_2$ requires C 40.15, H 3.56, N 7.80 %. UV/Vis (DMSO) $\lambda_{max}$ 258 ($3.16 \times 10^4$), 314 ($2.62 \times 10^4$), 388 ($6.97 \times 10^3$) nm ($M^{-1}\,cm^{-1}$). $\tilde{\nu}_{max}$ (MeOH) 2060, 1991, 1635, 1622 $cm^{-1}$. $m/z$ (orbitrap) 1077.9 $[M]^+$.

### *4.11. X-ray crystallography*

For each sample, crystals were suspended in oil, and one was mounted on a glass fibre and fixed in the cold nitrogen stream of the diffractometer. Data were collected using Mo-K$\alpha$ ($\lambda$ = 0.710 73 Å) radiation using an Oxford Diffraction Xcalibur-3 CCD diffractometer equipped with a graphite monochromator (**2a**·MeCN and **2d**·MeCN) or a Rigaku Saturn724+ diffractometer equipped with confocal mirrors (all others), and were processed using CrysAlisPro (**2a**·MeCN and **2d**·MeCN) [49].) or CrystalClear-SM Expert (all others) [50]. Structures were determined using a dual-space approach in SHELXT [51] and refined by

full-matrix least-squares methods on $F^2$ in SHELXL [51]. Non-hydrogen atoms were refined with anisotropic thermal parameters. The nitrogen-bound hydrogen atoms were located in the Fourier difference map and freely refined; all other hydrogen atoms were included in idealized positions and their $U_{iso}$ values were set to ride on the $U_{eq}$ values of the parent atom.

**Acknowledgements**

MAW thanks the University of East Anglia for funding. The authors thank the EPSRC UK National Mass Spectrometry Facility at Swansea University for mass spectrometry data and the EPSRC UK National Crystallography Service at the University of Southampton for the collection of the crystallographic data [52]. The authors thank Tyler Wooldridge for assistance in establishing the TNF assay protocol, Professor Chris Pickett for helpful discussions and a referee for useful comments.

**References**

[1] U. Schatzschneider, Photocorms: Light-triggered release of carbon monoxide from the coordination sphere of transition metal complexes for biological applications, Inorg. Chim. Acta 374 (1) (2011) 19–23. doi:10.1016/j.ica.2011.02.068.

[2] R. D. Rimmer, A. E. Pierri, P. C. Ford, Photochemically activated carbon monoxide release for biological targets. toward developing air-stable photocorms labilized by visible light, Coord. Chem. Rev. 256 (15-16) (2012) 1509–1519. doi:10.1016/j.ccr.2011.12.009.

[3] S. H. Heinemann, T. Hoshi, M. Westerhausen, A. Schiller, Carbon monoxide – physiology, detection and controlled release, Chem. Commun. 50 (28) (2014) 3644–3360. doi:10.1039/c3cc49196j.

[4] J. Marhenke, K. Trevino, C. Works, The chemistry, biology and design of photochemical co releasing molecules and the efforts to detect co for biological applications, Coord. Chem. Rev. 306 (2) (2015) 533–543. doi:10.1016/j.ccr.2015.02.017.

[5] U. Schatzschneider, Novel lead structures and activation mechanisms for co-releasing molecules (corms), Br. J. Pharmacol. 172 (6) (2014) 1638–1650. doi:10.1111/bph.12688.

[6] M. A. Wright, J. A. Wright, Photocorms: Co release moves into the visible, Dalton Trans. 45 (16) (2016) 6801–6811. doi:10.1039/c5dt04849d.

[7] M. N. Pinto, P. K. Mascharak, Light-assisted and remote delivery of carbon monoxide to malignant cells and tissues: Photochemotherapy in the spotlight, J. Photochem. Photobiol. C Photochem. Rev. 42 (2020) 100341. doi:10.1016/j.jphotochemrev.2020.100341.

[8] L. E. Otterbein, F. H. Bach, J. Alam, M. Soares, H. T. Lu, M. Wysk, R. J. Davis, R. A. Flavell, A. M. Choi, Carbon monoxide has anti-inflammatory effects involving the mitogen-activated protein kinase pathway, Nat. Med. 6 (4) (2000) 422–428. doi:10.1038/74680.

[9] R. Motterlini, R. Foresti, Biological signaling by carbon monoxide and carbon monoxide-releasing molecules, Am. J. Physiol. Cell. Physiol. 312 (3) (2017) C302–C313. doi:10.1152/ajpcell.00360.2016.

[10] M. A. Wright, T. Wooldridge, M. A. O'Connell, J. A. Wright, Ferracyclic carbonyl complexes as anti-inflammatory agents, Chem. Commun. 56 (31) (2020) 4300–4303. doi:10.1039/D0CC01449D.

[11] C. S. Jackson, S. Schmitt, Q. P. Dou, J. J. Kodanko, Synthesis, characterization, and reactivity of the stable iron carbonyl complex [fe(co)(n4py)](clo)2: Photoactivated carbon monoxide release, growth inhibitory activity, and peptide ligation, Inorg. Chem. 50 (12) (2011) 5336–5338. doi:10.1021/ic200676s.

[12] R. Kretschmer, G. Gessner, H. Görls, S. H. Heinemann, M. Westerhausen, Dicarbonyl-bis(cysteamine)iron(ii): A light induced carbon monoxide releasing molecule based on iron (corm-s1), J. Inorg. Biochem. 105 (1) (2011) 6–9. doi:10.1016/j.jinorgbio.2010.10.006.

[13] R. Motterlini, J. E. Clark, R. Foresti, P. Sarathchandra, B. E. Mann, C. J. Green, Carbon monoxide-releasing molecules: Characterization of biochemical and vascular activities, Circ. Res. 90 (2) (2002) 17–24. doi:10.1161/hh0202.104530.

[14] J. Marhenke, A. E. Pierri, M. Lomotan, P. L. Damon, P. C. Ford, C. Works, Flash and continuous photolysis kinetic studies of the iron–iron hydrogenase model $(\mu-\text{pdt})[\text{Fe(CO)}_3]_2$ in different solvents, Inorg. Chem. 50 (23) (2011) 11850–11852. doi:10.1021/ic201523r.

[15] H. T. Poh, B. T. Sim, T. S. Chwee, W. K. Leong, W. Y. Fan, The dithiolate-bridged diiron hexacarbonyl complex $\text{Na}_2[(\mu-\text{SCH}_2\text{CH}_2\text{COO})\text{Fe(CO)}_3]_2$ as a water-soluble photocorm, Organometallics 33 (4) (2014) 959–963. doi:10.1021/om401013a.

[16] M. A. Gonzalez, S. J. Carrington, N. L. Fry, J. L. Martinez, P. K. Mascharak, Syntheses, structures, and properties of new manganese carbonyls as photoactive co-releasing molecules: Design strategies that lead to co photolability in the visible region, Inorg. Chem. 51 (21) (2012) 11930–11940. doi:10.1021/ic3018216.

[17] M. A. Gonzalez, M. A. Yim, S. Cheng, A. Moyes, A. J. Hobbs, P. K. Mascharak, Manganese carbonyls bearing tripodal polypyridine ligands as photoactive carbon monoxide-releasing molecules, Inorg. Chem. 51 (1) (2012) 601–608. doi:10.1021/ic2021287.

[18] M. A. Gonzalez, S. J. Carrington, I. Chakraborty, M. M. Olmstead, P. K. Mascharak, Photoactivity of mono- and dicarbonyl complexes of ruthenium(ii) bearing an n,n,s-donor ligand: Role of ancillary ligands on the capacity of co photorelease, Inorg. Chem. 52 (19) (2013) 11320–11331. doi:10.1021/ic4016004.

[19] S. J. Carrington, I. Chakraborty, P. K. Mascharak, Rapid co release from a mn(i) carbonyl complex derived from azopyridine upon exposure to visible

light and its phototoxicity toward malignant cells, Chem. Commun. 49 (96) (2013) 11254–11256. doi:10.1039/c3cc46558f.

[20] I. Chakraborty, S. J. Carrington, P. K. Mascharak, Photodelivery of co by designed photocorms: Correlation between absorption in the visible region and metal-co bond labilization in carbonyl complexes, ChemMedChem 9 (6) (2014) 1266–1274. doi:10.1002/cmdc.201402007.

[21] S. J. Carrington, I. Chakraborty, J. M. L. Bernard, P. K. Mascharak, Synthesis and characterization of a "turn-on" photocorm for trackable co delivery to biological targets, ACS Med. Chem. Lett. 5 (12) (2014) 1324–1328. doi:10.1021/ml500399r.

[22] M. A. Gonzales, H. Han, A. Moyes, A. Radinos, A. J. Hobbs, N. Coombs, S. R. J. Oliver, P. K. Mascharak, Light-triggered carbon monoxide delivery with al-MCM-41-based nanoparticles bearing a designed manganese carbonyl complex, J. Mater. Chem. B 2 (15) (2014) 2107–2113. doi:10.1039/c3tb21309a.

[23] I. Chakraborty, S. J. Carrington, P. K. Mascharak, Design strategies to improve the sensitivity of photoactive metal carbonyl complexes (photocorms) to visible light and their potential as co-donors to biological targets, Acc. Chem. Res. 47 (8) (2014) 2603–2611. doi:10.1021/ar500172f.

[24] M. A. Gonzales, P. K. Mascharak, Photoactive metal carbonyl complexes as potential agents for targeted co delivery, J. Inorg. Biochem. 133 (2014) 127–135. doi:10.1016/j.jinorgbio.2013.10.015.

[25] S. J. Carrington, I. Chakraborty, P. K. Mascharak, Exceptionally rapid co release from a manganese(i) tricarbonyl complex derived from bis(4-chlorophenylimino)acenaphthene upon exposure to visible light, Dalton Trans. 44 (2015) 13828–13834. doi:10.1039/c5dt01007a.

[26] I. Chakraborty, S. J. Carrington, J. Hauser, S. R. J. Oliver, P. K. Mascharak, Rapid eradication of human breast cancer cells through trackable light-triggered CO delivery by mesoporous silica nanoparticles packed with a designed photoCORM, Chem. Mater. 27 (24) (2015) 8387–8397. doi:10.1021/acs.chemmater.5b03859.

[27] R. Mede, V. P. Lorett-Velásquez, M. Klein, H. Görls, M. Schmitt, G. Gessner, S. H. Heinemann, J. Popp, M. Westerhausen, Carbon monoxide release properties and molecular structures of phenylthiolatomanganese(i) carbonyl complexes of the type [(oc) 4 mn(mu-s-aryl)] 2, Dalton Trans. 44 (7) (2015) 3020–3033. doi:10.1039/c4dt03567d.

[28] S. J. Carrington, I. Chakraborty, J. M. L. Bernard, P. K. Mascharak, A theranostic two-tone luminescent PhotoCORM derived from re(i) and (2-pyridyl)-benzothiazole: Trackable CO delivery to malignant cells, Inorg. Chem. 55 (16) (2016) 7852–7858. doi:10.1021/acs.inorgchem.6b00511.

[29] M. Tinajero-Trejo, N. Rana, C. Nagel, H. E. Jesse, T. W. Smith, L. K. Wareham, M. Hippler, U. Schatzschneider, R. K. Poole, Antimicrobial activity of the manganese photoactivated carbon monoxide-releasing molecule $[Mn(CO)_3(tpa{-}\kappa_3N)]^+$ against a pathogenic escherichia coli that

causes urinary infections, Antioxid. Redox Signaling 24 (14) (2016) 765–780. doi:10.1089/ars.2015.6484.

[30] I. Chakraborty, J. Jimenez, W. M. C. Sameera, M. Kato, P. K. Mascharak, Luminescent re(i) carbonyl complexes as trackable PhotoCORMs for CO delivery to cellular targets, Inorg. Chem. 56 (5) (2017) 2863–2873. doi:10.1021/acs.inorgchem.6b02999.

[31] J. Jimenez, I. Chakraborty, A. Dominguez, J. Martinez-Gonzalez, W. M. C. Sameera, P. K. Mascharak, A luminescent manganese PhotoCORM for CO delivery to cellular targets under the control of visible light, Inorg. Chem. 57 (4) (2018) 1766–1773. doi:10.1021/acs.inorgchem.7b02480.

[32] M. N. Pinto, I. Chakraborty, J. Jimenez, K. Murphy, J. Wenger, P. K. Mascharak, Therapeutic potential of two visible light responsive luminescent photocorms: Enhanced cellular internalization driven by lipophilicity, Inorg. Chem. 58 (21) (2019) 14522–14531. doi:10.1021/acs.inorgchem.9b02121.

[33] B. Kawahara, L. Gao, W. Cohn, J. P. Whitelegge, S. Sen, C. Janzen, P. K. Mascharak, Diminished viability of human ovarian cancer cells by antigen-specific delivery of carbon monoxide with a family of photoactivatable antibody-photoCORM conjugates, Chem. Sci. 11 (2020) 467–473. doi:10.1039/C9SC03166A.

[34] A. E. Pierri, A. Pallaoro, G. Wu, P. C. Ford, A luminescent and biocompatible photocorm, J. Am. Chem. Soc. 134 (44) (2012) 18197–18200. doi:10.1021/ja3084434.

[35] C. Bischof, T. Joshi, A. Dimri, L. Spiccia, U. Schatzschneider, Synthesis, spectroscopic properties, and photoinduced co-release studies of functionalized ruthenium(ii) polypyridyl complexes: Versatile building blocks for development of corm–peptide nucleic acid bioconjugates, Inorg. Chem. 52 (16) (2013) 9297–9308. doi:10.1021/ic400746n.

[36] S. Yang, M. Chen, L. Zhou, G. Zhang, Z. Gao, W. Zhang, Photoactivated CO-releasing molecules (PhotoCORMs) of robust sawhorse scaffolds [$\mu_2-OOCR_1$, $\eta_1-nh_2chr_2(c{\equiv}o]och_3$, $Ru(I)_2CO_4$], Dalton Trans. 45 (9) (2016) 3727–3733. doi:10.1039/c5dt04479k.

[37] A. M. Mansour, RuII -carbonyl photoCORMs with n,n -benzimidazole bidentate ligands: Spectroscopic, lysozyme binding affinity, and biological activity evaluation, Eur. J. Inorg. Chem. 2018 (7) (2018) 852–860. doi:10.1002/ejic.201701341.

[38] A. M. Mansour, O. R. Shehab, {ru(CO)x}-core terpyridine complexes: Lysozyme binding affinity, DNA and photoinduced carbon monoxide releasing properties, J. Photochem. Photobiol. A: Chem. 364 (2018) 406–414. doi:10.1016/j.jphotochem.2018.06.026.

[39] M. Kubeil, R. R. Vernooij, C. Kubeil, B. R. Wood, B. Graham, H. Stephan, L. Spiccia, Studies of carbon monoxide release from ruthenium(II) bipyridine carbonyl complexes upon UV-light exposure, Inorg. Chem. 56 (10) (2017) 5941–5952. doi:10.1021/acs.inorgchem.7b00599.

[40] M. Nonoyama, Ruthenium(II) complexes derived from 2-(methylamino)pyridine, Inorg. Chim. Acta 115 (2) (1986) 169–172. doi:10.1016/s0020-1693(00)84409-6.

[41] C. K. Barik, R. Ganguly, Y. Li, W. K. Leong, Structural mimics of the [fe]-hydrogenase: A complete set for group VIII metals, Inorg. Chem. 57 (12) (2018) 7113–7120. doi:10.1021/acs.inorgchem.8b00838.

[42] C. K. Barik, R. Ganguly, Y. Li, C. Przybylski, M. Salmain, W. K. Leong, Embedding a ruthenium-based structural mimic of the [Fe]-hydrogenase cofactor into papain, Inorg. Chem. 57 (19) (2018) 12206–12212. doi:10.1021/acs.inorgchem.8b01835.

[43] I. F. Barnard, J. A. Elvidge, Heterocyclic imines and amines. part 18. conversion of o-cyanobenzyl cyanide into isoquinoline, benzylisoquinoline, and azachrysene products, J. Chem. Soc., Perkin Trans. 1 (1983) 1137doi:10.1039/p19830001137.

[44] J. Reed, M. J. Stephenson, K. Miettinen, B. Brouwer, A. Leveau, P. Brett, R. J. Goss, A. Goossens, M. A. O'Connell, A. Osbourn, A translational synthetic biology platform for rapid access to gram-scale quantities of novel drug-like molecules, Metab. Eng. 42 (2017) 185–193. doi:10.1016/j.ymben.2017.06.012.

[45] R. Steel, J. Cowan, E. Payerne, M. A. O'Connell, M. Searcey, Anti-inflammatory effect of a cell-penetrating peptide targeting the nrf2/keap1 interaction, ACS Med. Chem. Lett. 3 (5) (2012) 407–410. doi:10.1021/ml300041g.

[46] F. Calderazzo, F. L'Eplattenier, Pentacarbonyls of ruthenium and osmium. i. infrared spectra andreactivity, Inorg. Chem. 6 (6) (1967) 1220–1224. doi:10.1021/ic50052a033.

[47] W. R. Hastings, M. R. Roussel, M. C. Baird, Mechanism of the conversion of $[Ru(CO)_5]$ into $[Ru_3(CO)_{12}]$, J. Chem. Soc., Dalton Trans. (1) (1990) 203. doi:10.1039/dt9900000203.

[48] N. Floyd, B. Vijayakrishnan, J. R. Koeppe, B. G. Davis, Thiyl glycosylation of olefinic proteins: S-linked glycoconjugate synthesis, Angew. Chem. Int. Ed. 48 (42) (2009) 7798–7802. doi:10.1002/anie.200903135.

[49] Agilent Technologies Ltd., Yarnton, United Kingdom, CrysAlisPro (2012).

[50] Rigaku Corporation, Tokyo, Japan, CrystalClear-SM Expert (2012).

[51] G. M. Sheldrick, A short history of shelx, Acta Cryst. A 64 (1) (2008) 112–122. doi:10.1107/s0108767307043930.

[52] S. J. Coles, P. A. Gale, Changing and challenging times for service crystallography, Chem. Sci. 3 (2012) 683–689. doi:10.1039/C2SC00955B.